Applied Surface Science 265 (2013) 358–362

Contents lists available at SciVerse ScienceDirect

Applied Surface Science

journal homepage: www.elsevier.com/locate/apsusc

Quantification of strain through linear dichroism in the Si 1s edge X-ray absorption spectra of strained $Si_{1-x}Ge_x$ thin films

W. Cao [a,1], M. Masnadi [a], S. Eger [a], M. Martinson [a], Q.-F. Xiao [b], Y.-F. Hu [b], J.-M. Baribeau [c], J.C. Woicik [d], A.P. Hitchcock [e], S.G. Urquhart [a,*]

[a] Department of Chemistry, University of Saskatchewan, Saskatoon, SK S7N 5C9, Canada
[b] Canadian Light Source, University of Saskatchewan, Saskatoon, SK S7N 0X4, Canada
[c] National Research Council, Ottawa, ON K1A 0R6, Canada
[d] Ceramics Division, National Institute of Standards and Technology, Gaithersburg, MD 20899, United States
[e] Brockhouse Institute for Materials Research, McMaster University, Hamilton, ON L8S 4M1, Canada

ARTICLE INFO

Article history:
Received 17 July 2012
Received in revised form 22 October 2012
Accepted 3 November 2012
Available online 9 November 2012

Keywords:
Strain
Silicon germanium alloys
X-ray absorption spectroscopy
NEXAFS

ABSTRACT

We have quantitatively measured the angle dependence in the Silicon 1s X-ray absorption spectra of strained $Si_{1-x}Ge_x$ thin films prepared by epitaxial growth on Si(1 0 0) substrates, through surface sensitive total electron yield detection. The linear dichroism difference extracted from these angle dependent X-ray absorption spectra is proportional to the degree of strain, as measured separately by Raman spectroscopy. This quantitative relationship provides a means to measure the compressive strain in $Si_{1-x}Ge_x$ thin films. This strain-dependent X-ray absorption spectroscopy has the potential to realize a semiconductor strain metrology through high spatial resolution X-ray spectromicroscopy.

© 2012 Elsevier B.V. All rights reserved.

1. Introduction

As an important material in the microelectronics industry, strained $Si_{1-x}Ge_x$ alloy films prepared by epitaxial growth, have been engineered to produce high frequency transceivers [1], quantum well infrared photodetectors [2], and nanoscale CMOS [3] and light-emitting [4] devices. The electronic structure of epitaxially grown $Si_{1-x}Ge_x$ alloys is dependent on the composition, crystallographic orientation of the substrate as well as the degree of strain [5]. Strain can be engineered to increase electron mobility [6]. The degree of strain depends on film composition, thickness, and processing history [7–10]. Films that are thicker than a composition dependent critical thickness [11] relax through misfit dislocations [8].

Measurement of the degree of strain in $Si_{1-x}Ge_x$ alloys is important for optimizing the structure and properties of $Si_{1-x}Ge_x$ devices. Measurement of the sample strain with high lateral spatial resolution – down to the individual gate length scale – remains a challenge for the development and optimization of strained $Si_{1-x}Ge_x$ devices, as well other strained semiconductor materials. Strain distributions in $Si_{1-x}Ge_x$ alloys have been studied by transmission electron microscopy (TEM) [12,13], X-ray diffraction (XRD) [14], and Raman microscopy [15]. The spatial resolution of Raman and micro-XRD techniques can reach ~0.3 μm [16], while AFM-induced enhanced Raman scattering has provided sub-100 nm spatial resolution on $Si_{1-x}Ge_x$ quantum dots [17]. There is a need to go smaller: the fourth generation of high speed SiGe heterojunction bipolar transistor (HBT) and bipolar complementary metal oxide semiconductor (BiCMOS) technology will have gate lengths below 90 nm [18]. Experimental measurement of strain in $Si_{1-x}Ge_x$ thin films, down the scale of individual devices and below the scale of Raman and XRD, remains an important analytical challenge.

In this work, we study the angle dependence in the Si 1s X-ray absorption spectra (XAS) of strained $Si_{1-x}Ge_x$ thin films. The shape of the fine structure at the onset of the Si 1s XAS shows a strong dependence on $Si_{1-x}Ge_x$ composition; the linear dichroism (LD) of these features shows a dependence on the degree of strain. This has been studied earlier [19,20] but a quantitative relationship between the magnitude of the LD and the strain has not been determined previously. The use the LD-XAS difference (the difference between spectra recorded with horizontal and vertical polarization) largely removes the composition variation from the spectra, isolating the effect of strain. This LD-XAS can therefore be used to reveal anisotropic states associated with strain-induced distortions [20]. We correlate the strength of the LD-XAS effect with strain, independently measured by Raman spectroscopy, to obtain

* Corresponding author.
E-mail addresses: wei.cao@oulu.fi (W. Cao), stephen.urquhart@usask.ca (S.G. Urquhart).
[1] Current address: Department of Physics, University of Oulu, FIN-90014 Finland.

0169-4332/$ – see front matter © 2012 Elsevier B.V. All rights reserved.
http://dx.doi.org/10.1016/j.apsusc.2012.11.012

Table 1
Summary of $Si_{1-x}Ge_x$ alloy sample composition, thickness, strain and the integrated absolute value of the linear dichroism difference.

NRC sample code	Composition from prep. (x)	Thickness (nm)	Composition from XPS (x)	Composition from Raman (x)	Degree of strain (from Raman%)	Integral (eV*Int.)
929	0.12	105	0.31	0.098(8)	−0.29(7)	0.054
930	0.20	180	0.18	0.179(5)	−0.66(1)	0.083
1474	0.24	100	0.26	0.206(5)	−0.87(4)	0.101
1632	0.39	250	0.46	0.367(3)	−0.34(2)	0.047
1201	0.44	300	0.47	0.404(40)	−0.08(3)	0.029

a quantitative relationship. This LD-XAS has the potential for use for quantitative strain mapping at the scale of individual gates (sub-100 nm spatial scale), through X-ray linear dichroism microscopy (XLDM) with an X-ray photoelectron emission microscope [21].

2. Experiments

2.1. $Si_{1-x}Ge_x$ alloy samples

$Si_{1-x}Ge_x$ thin films that vary in composition and thicknesses were employed for the Si 1s X-ray absorption measurements. $Si_{1-x}Ge_x$ alloy films were grown by molecular-beam epitaxy (MBE) using electron beam evaporators and solid Si and Ge sources at the Institute for Microstructural Sciences National Research Council (NRC-IMS) of Canada. Base chamber pressure was typically $< 2 \times 10^{-10}$ mbar, with an order of magnitude increase during growth. Samples were grown on commercial [1 0 0] oriented Si wafers, which were heated to 500 °C during the growth. More details of the sample information can be found in Aubry et al. [22]. The sample composition (estimated from the preparation conditions, and determined by Raman and XPS) and the film thickness are listed in Table 1.

2.2. Characterization of $Si_{1-x}Ge_x$ thin films

Composition estimates provided by the growth conditions were verified by X-ray photoemission spectroscopy (XPS) and Raman spectroscopy; Raman spectroscopy is also used to determine the degree of strain. Atomic force microscopy (AFM) was used to verify that the films are uniform with no apparent island formation. Details of the sample composition and degree of strain will be discussed in Section 3.

Raman spectra were acquired on the Raman microscope at the Saskatchewan Structural Sciences Centre, using the 514.5 nm radiation from an Ar^+ laser. The position of the Si–Si and the Si–Ge bands was determined by fitting these lines with an asymmetric Gaussian function (Eq. (1) in Ref. [23]). The composition (x) and strain (ε) from the Raman data were calculated using the standard formulas (Eqs. (12) and (13) of Perova et al. [23]). These data are tabulated in Table 1. Raman results are expected to average the strain in the entire $Si_{1-x}Ge_x$ thin film, while TEY-NEXAFS are somewhat more sensitive to the near-surface signal (∼70 nm sampling depth, according to Ref. [24]).

The $Si_{1-x}Ge_x$ composition was further verified by XPS. XPS data was collected using an XPS spectrometer at the Alberta Center for Surface Engineering and Science. A monochromatic Al Kα X-ray source was used, and high resolution Si 2p, Ge 3d, and C 1s spectra were collected (20 eV pass energy; 0.1 eV step size; 200 ms dwell time). Spectra were calibrated to the adventitious C 1s line at 284.8 eV and a Shirley type background subtraction was used to account for energy loss due to inelastic scattering [25,26]. Manual regions were created for the Si 2p and the Ge 3d spectra, which included the oxide peaks for both Si and Ge [27,28]. XPS composition results are listed in Table 1.

2.3. Polarization dependent X-ray absorption spectroscopy

The polarization dependent XAS measurements were carried out using the Soft X-ray Microcharacterization Beamline (SXRMB) [29], a bending magnet beamline at the Canadian Light Source Saskatoon, Canada covering the "tender" X-ray region (1.5–10 keV). An InSb(1 1 1) monochromator was used, and the degree of horizontal linear polarization is estimated to be 80%, from a measurement of the intensity as a function of horizontal slit setting. A typical flux of the beam is $>10^{11}$ ph/s with the energy resolving power of $\sim 4 \times 10^3$ at the Si 1s edge.

Measurements were performed on the Si(1 0 0) face of a commercially available Si single crystal and five $Si_{1-x}Ge_x$ alloy samples (see Table 1). The native oxide was first removed by a short etch (5 s in a 10% HF solution, followed by rinsing with distilled water). Each sample was mounted so that the photon beam strikes the sample at a glancing angle of $18^\circ \pm 2^\circ$ ($72^\circ \pm 2^\circ$ relative to the surface normal), providing a constant ratio of the surface/bulk sensitivity at all sample rotation angles. The sample can be rotated about an axis parallel to the photon propagation direction. In the horizontal geometry, the electric field vector is oriented in the sample plane, while in vertical geometry, the electric field vector is nearly normal to the sample surface. Spectra recorded in these geometries are defined as the horizontal and vertical XAS, respectively. An energy range from 1820 to 1910 eV was selected for the XAS measurement, with energy step of 0.1 eV at the peak region.

Total electron yield (TEY) was recorded as a sample drain current using a high precision picoammeter. At the Si 1s edge, the TEY sampling depth was estimated to be ∼70 nm [24]. For normalization, the incoming flux was monitored using an ion chamber located upstream in the beam path. Sufficient dwell time and scans were selected for each sample to provide good statistics.

3. Results and discussion

Composition, thickness and strain data for the five $Si_{1-x}Ge_x$ are provided in Table 1. With the exception of the XPS measurement for sample 929, the composition measurements are within a few percent. The Raman values are all slightly lower than the values expected from the sample preparation, perhaps reflecting a small offset in evaporation source calibration. The XPS values show the same composition trend, but vary more widely.

The difference between the horizontal and vertical XAS of strained $Si_{1-x}Ge_x$ has been hypothesized to be proportional to the degree of strain [20]. To verify this, the Si 1s XAS of unstrained crystalline Si(1 0 0) was first examined. The normalized horizontal and vertical spectra overlap very closely in the measured energy region, with a small difference (<0.4%) in the energy region of the strong white line feature (1839.8–1845.8 eV). This residual may represent an effect of the surface anisotropy on the Si(1 0 0) surface. The small LD-XAS difference is therefore considered as the "strain detection limit" in these experiments.

The LD-XAS signals measured for the strained $Si_{1-x}Ge_x$ samples were then correlated with the degree of the strain. A typical

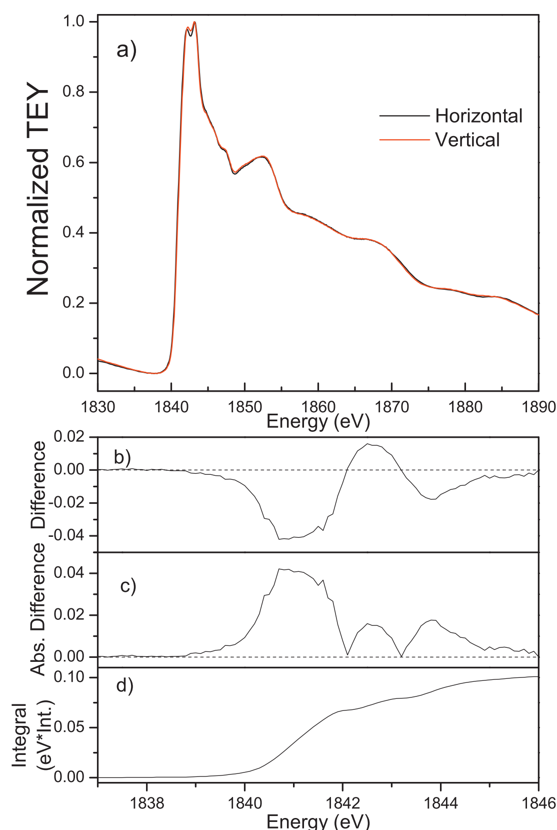

Fig. 1. (a) Silicon 1s X-ray absorption spectra of sample 1474 (100 nm $Si_{0.76}Ge_{0.24}$ alloy), recorded with total electron yield, with horizontal and vertical polarization. These spectra have been normalized so that the maximum intensity is set to 1.0 and the minimum intensity is set to 0.0; see Section 2.3 for a description of the sample geometry and data processing; (b) the difference of vertical spectra and horizontal polarized X-ray absorption spectra; (c) the absolute value of this difference; and (d) the integration of the absolute value to the energy.

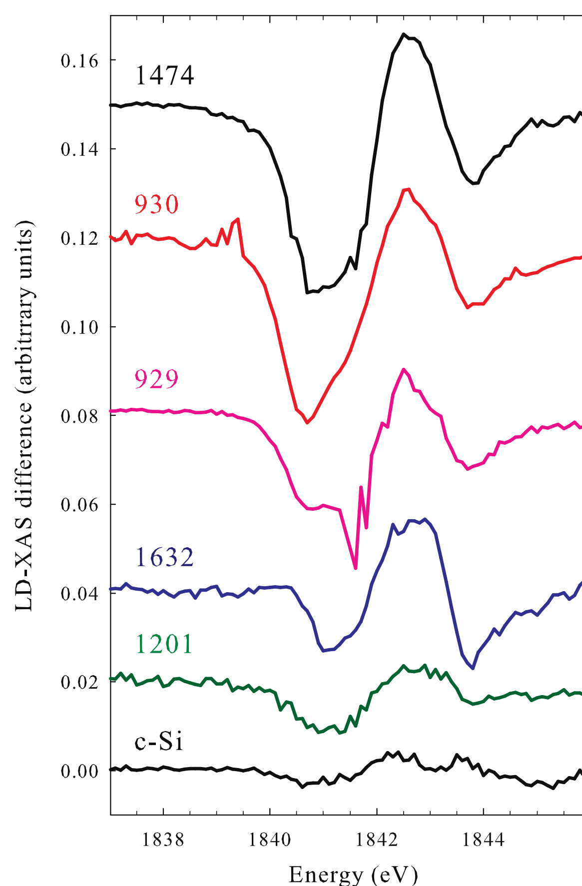

Fig. 2. The LD-XAS differences for the samples investigated in the energy region of interest, plotted in the order of strain, ε (lowest on the bottom), and the energy range corresponds to that used for integration.

LD-XAS for the $Si_{1-x}Ge_x$ thin film, sample code 1474 (nominal Ge composition: 0.24; thickness: 100 nm) is presented in Fig. 1a after normalization, where the strongest and weakest signals were set to 1.0 and 0.0, respectively. The LD-XAS difference spectrum for sample 1474 derived in this fashion is also shown in Fig. 1b. The pre-edge (1830–1838 eV) and the far continuum (above 1855 eV) signals in the horizontal and vertical spectra overlap, while clear differences due to linear dichroism are observed in the intense white line of the Si 1s edge spectrum (1839–1844 eV region). The white line of silicon and SiGe alloys consists of "rabbit ear" structures; two peaks closely separated in energy that arise from conduction-band splitting [30]. The separation and relative intensity depends on composition. Features that appear at higher energy are attributed to multiple scattering effects (~5 eV above the edge) [31], while features above 1858 eV are attributed to longer range crystalline order [20,22]. To evaluate the strain, we focus on the region from 1837 to 1846 eV, where LD differences are up to ~10 times larger than the differences found in crystalline-Si.

The LD-XAS differences for the other samples were similar to that for sample 1474. The LD-XAS difference spectra for all samples are presented in Fig. 2, in order to compare the magnitude and character of these differences. Small glitch points, originating from a small (<1%) variation in the intensity of single data points, have been edited out of this plot for clarity; the original LD-difference spectra used for data analysis are presented in the supplementary data. It is clear that the LD difference increases with the degree of strain, ε.

The method of data normalization used in this work, where the minimum intensity of the horizontal and vertical spectra was set to 0.0, and the maximum intensity of these spectra was set to 1.0, was found to be superior to commonly used normalization methods (such as that discussed in Ref. [32]). Commonly, spectra are background subtracted and normalized in the continuum (above near-edge features) to an atomic cross-section [33] or to a constant. However, the background subtraction step can add uncertainty to the slope in the continuum, introducing artificial differences between the horizontal and vertical polarized spectra. The normalization method used in this work can be automated. Previously, small linear dichroism signals have been used for quantitative orientation mapping in semi-crystalline organic polymers such as spider dragline silk [34]. Similarly, a strain metrology, using a pixel-by-pixel spectra processing of the linear dichroism in X-ray microscopy data, is proposed for strained polymers.

3.1. Qualification of the XAS-LD to the strain

It is crucial to quantify the LD-XAS signal in order to develop this phenomenon as the basis for a strain metrology. Visual inspection suggests that the LD-XAS difference scales with the degree of strain [35]. A quantitative evaluation is required to establish an analytical measure of strain. Composition differences will shift the XAS as well as the LD-XAS difference spectra [20,36], so the intensity of a single transition (or a small set of features) cannot be used easily to measure strain in samples with variable composition. As the LD-XAS spectra have positive and negative values, we convert the LD-XAS difference spectrum to absolute value scale (shown in Fig. 1c) and then calculate the area under this curve (integral shown

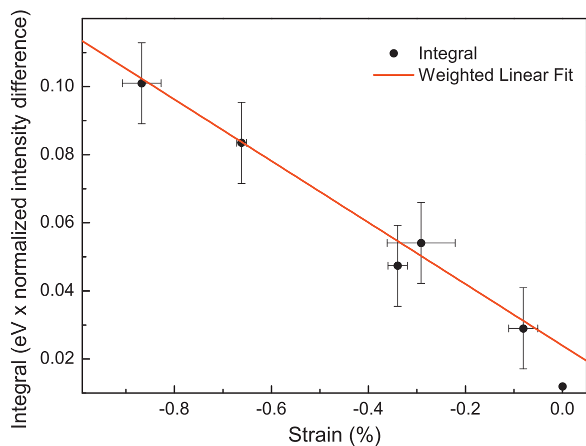

Fig. 3. Integral of the absolute differences to the energy as a function of strain, ε. The data were further fitted with a weighted linear function (red line; $y = mx + b$, where $m = -9.13739 \pm 1.8987$; $b = 2.295 \times 10^{-2} \pm 1.004 \times 10^{-2}$; reliability $r^2 = 0.9811$). (For interpretation of the references to color in this figure legend, the reader is referred to the web version of the article.)

in Fig. 1d; 1837–1846 eV). The numerical integral was employed to calculate the area within the energy range. The method was applied to the LD-XAS signals of the other 4 samples as well as c-Si. The corresponding integral value for c-Si was used as the error for the integrals of the LD-XAS signals from the $Si_{1-x}Ge_x$ samples. The values of the integrated LD-XAS signal for the 5 samples are listed in the last column of Table 1 and also plotted as a function of the strain in Fig. 3. The magnitude of the quantitative LD-XAS signal increases linearly with the strain, within the estimated uncertainties from the Raman analysis. Taking the errors as weights, a linear fit was applied to the data and is shown in Fig. 3.

The degree of strain and the integrated LD-XAS difference are proportional to each other. The use of the integral is essential, as the shape of the LD-XAS signal changes with $Si_{1-x}Ge_x$ composition [20]. Evaluating the integral of the absolute value of the LD-XAS signal desensitizes the method to the compositionally dependent shape variations. The LD-XAS difference at any single energy is not likely to be meaningful and would require constrained multiline fitting to process [20], unlike, for example, LD-XAS studies in oriented anisotropic organic materials [37].

The magnitude of the integral – and thus the strain – in an arbitrary $Si_{1-x}Ge_x$ sample with an unknown degree of compressive strain can be measured by this approach. Using Fig. 3 as a calibration curve, the value of the integrated LD-XAS can be determined to quantitatively estimate the degree of strain.

For this calibration, the LD-XAS differences are compared to strain measurements determined separately by Raman spectroscopy. It is important to consider the differences in depth sensitivity of these methods. XAS, measured by TEY detection at the Si 1s edge, has a sampling depth of ~70 nm [24]. In contrast, Raman should integrate the strain of the entire $Si_{1-x}Ge_x$ thin film (100–300 nm thick, as shown in Table 1). However, the mechanisms of strain relaxation and defect propagation in strained $Si_{1-x}Ge_x$ thin films [11] suggest that the strain will be the similar throughout the $Si_{1-x}Ge_x$ thin film. Therefore, the Raman and LD-XAS strain measurements are comparable.

At the present level of standard evaluation, this approach shown in Fig. 3 should give a value of the strain with an uncertainty of 5%. While convergent beam electron diffraction provides higher precision [13], the X-PEEM method requires much less sample preparation and wide areas can be surveyed easily, and used as a strain metrology.

4. Conclusion

The linear dichroism of Si 1s edge X-ray absorption spectra (LD-XAS) of strained SiGe thin films grown epitaxially on a c-Si(1 0 0) substrate has been measured. The integrated absolute LD-XAS from 1838 to 1846 eV has been shown to be a quantitative measure of the strain for these $Si_{1-x}Ge_x$ thin films. The integral of the absolute value of the LD-XAS difference linearly varies with the degree of the strain in these compressively strained $Si_{1-x}Ge_x$ systems. These results have the potential for use for quantitative strain mapping at the scale of individual gates (sub-100 nm spatial scale) by X-ray linear dichroism microscopy (XLDM) with an X-ray photoelectron emission microscope [21], where strain dependent spectra can be acquired with <50 nm lateral spatial resolution.

Acknowledgements

Research described in this paper was performed at the Canadian Light Source, the Saskatchewan Structural Sciences Centre and the Alberta Center for Surface Engineering and Science. The Canadian Light Source is supported by NSERC, NRC (Canada), CIHR, the Province of Saskatchewan, WED, and the University of Saskatchewan. The Saskatchewan Structural Sciences Centre is supported by the University of Saskatchewan, and the Alberta Center for Surface Engineering and Science is supported by the University of Alberta. This work is supported financially by an NSERC strategic research grant. WC is supported by the University of Oulu since January 2012. We thank Professor Andrew Grosvenor for his help with the XPS data analysis, and Dr. Jason Maley for help with Raman microscopy.

Appendix A. Supplementary data

Supplementary data associated with this article can be found, in the online version, at http://dx.doi.org/10.1016/j.apsusc.2012.11.012.

References

[1] J.O. Plouchart, H. Ainspan, M. Soyuer, A. Ruehli, A fully-monolithic SiGe differential voltage-controlled oscillator for 5 GHz wireless applications, in: Radio Frequency Integrated Circuits (RFIC) Symposium, 2000. Digest of Papers 2000 IEEE, 2000, pp. 57–60.
[2] J.S. Park, R.P.G. Karunasiri, K.L. Wang, Applied Physics Letters 60 (1992) 103–105.
[3] C.L. Royer, Microelectronic Engineering 88 (2011) 1541–1548.
[4] N.D. Zakharov, V.G. Talalaev, P. Werner, A.A. Tonkikh, G.E. Cirlin, Applied Physics Letters 83 (2003) 3084–3086.
[5] Q.M. Ma, K.L. Wang, J.N. Schulman, Physical Review B 47 (1993) 1936–1953.
[6] M.L. Lee, E.A. Fitzgerald, M.T. Bulsara, M.T. Currie, A. Lochtefeld, Journal of Applied Physics 97 (2005) 011101–011128.
[7] K. Brunner, Reports on Progress in Physics 65 (2002) 27.
[8] P.M.J. Maree, J.C. Barbour, J.F. van der Veen, K.L. Kavanagh, C.W.T. Bulle-Lieuwma, M.P.A. Viegers, Journal of Applied Physics 62 (1987) 4413–4420.
[9] J.C. Bean, L.C. Feldman, A.T. Fiory, S. Nakahara, I.K. Robinson, Journal of Vacuum Science & Technology A: Vacuum, Surfaces, and Films 2 (1984) 436–440.
[10] J.C. Bean, Science 230 (1985) 127–131.
[11] R. People, J.C. Bean, Applied Physics Letters 47 (1985) 322–324.
[12] C.-P. Liu, J.M. Gibson, D.G. Cahill, T.I. Kamins, D.P. Basile, R.S. Williams, Physical Review Letters 84 (2000) 1958–1961.
[13] M. Cushley, Journal of Physics: Conference Series 126 (2008) 012086.
[14] I. Robinson, R. Harder, Nature Materials 8 (2009) 291–298.
[15] N. Hayazawa, M. Motohashi, Y. Saito, S. Kawata, Applied Physics Letters 86 (2005) 263114.
[16] I. De Wolf, V. Senez, R. Balboni, A. Armigliato, S. Frabboni, A. Cedola, S. Lagomarsino, Microelectronic Engineering 70 (2003) 425–435.
[17] Y. Ogawa, T. Toizumi, F. Minami, A.V. Baranov, Physical Review B 83 (2011) 081302.
[18] J.D. Cressler, The big picture, in: J.D. Cressler (Ed.), Silicon Heterostructure Handbook—Materials, Fabrication, Devices, Circuits, and Applications of SiGe and Si Strained-Layer Epitaxy, CRC Press, 2005, pp. 3–14.
[19] A.P. Hitchcock, T. Tyliszczak, P. Aebi, J.Z. Xiong, T.K. Sham, K.M. Baines, K.A. Mueller, X.H. Feng, J.M. Chen, B.X. Yang, Z.H. Lu, J.M. Baribeau, T.E. Jackman, Surface Science 291 (1993) 349–369.

[20] A.P. Hitchcock, T. Tyliszczak, P. Aebi, X.H. Feng, Z.H. Lu, J.-M. Baribeau, T. Jackman, Surface Science 301 (1994) 260.
[21] S.G. Urquhart, U.D. Lanke, J. Fu, International Journal of Nanotechnology 5 (2008) 1138–1170.
[22] J.C. Aubry, T. Tyliszczak, A.P. Hitchcock, J.-M. Baribeau, T.E. Jackman, Physical Review B 59 (1999) 12872.
[23] T.S. Perova, J. Wasyluk, K. Lyutovich, E. Kasper, M. Oehme, K. Rode, A. Waldron, Journal of Applied Physics 109 (2011) 033502–033511.
[24] M. Kasrai, W.N. Lennard, R.W. Brunner, G.M. Bancroft, J.A. Bardwell, K.H. Tan, Applied Surface Science 99 (1996) 303–312.
[25] M.W. Gaultois, A.P. Grosvenor, Journal of Materials Chemistry 21 (2011) 1829–1836.
[26] A.P. Grosvenor, R.G. Cavell, A. Mar, Chemistry of Materials 18 (2006) 1650–1657.
[27] Y.R. Xing, J.A. Wu, S.D. Yin, Surface Science 334 (1995) L705–L708.
[28] C. Chen, J. Liu, B. Yu, D. Zhu, Electronic Materials Letters 3 (2007) 63–67.
[29] Y.F. Hu, I. Coulthard, D. Chevrier, G. Wright, R. Igarashi, A. Sitnikov, B.W. Yates, E.L. Hallin, T.K. Sham, R. Reininger, AIP Conference Proceedings 1234 (2010) 343–346.
[30] J.C. Woicik, R.S. List, B.B. Pate, P. Pianetta, Solid State Communications 65 (1988) 685–688.
[31] A. Bianconi, A. Di Cicco, N.V. Pavel, M. Benfatto, A. Marcelli, C.R. Natoli, P. Pianetta, J. Woicik, Physical Review B 36 (1987) 6426–6433.
[32] A.P. Hitchcock, D.C. Mancini, Journal of Electron Spectroscopy and Related Phenomena 67 (1994) vii.
[33] B.L. Henke, E.M. Gullikson, J.C. Davis, Atomic Data and Nuclear Data Tables 54 (1993) 181–342.
[34] M.-E. Rousseau, D. Hernández Cruz, M.M. West, A.P. Hitchcock, M. Pézolet, Journal of the American Chemical Society 129 (2007) 3897–3905.
[35] J.C. Aubry, X-ray Absorption Fine Structure Spectroscopy of Thin Film SiGe Alloys, McMaster University, Hamilton, Ontario, 1996.
[36] W. Cao, M. Masnadi, L. Zuin, Y.-F. Hu, J.-M. Baribeau, J.C. Woicik, J.M. MacLeod, F. Rosei, A.P. Hitchcock, S.G. Urquhart, in preparation.
[37] J. Fu, S.G. Urquhart, The Journal of Physical Chemistry A 109 (2005) 11724–11732.